Dispersion Surfaces

15

CHAPTER PREVIEW

The analysis of Bloch waves we gave in the previous chapter is closely related to the classical analysis of waves that you've seen in solid-state physics or semiconductor theory. In semiconductors in particular, we often talk of indirect and direct band gaps. We use terms like conduction bands, valence bands, and Brillouin-zone boundaries (BZBs). We visualize these quantities by drawing diagrams of $E(\mathbf{k})$, the electron energy (which is a function of $\mathbf{k}$) versus $\mathbf{k}$, the wave vector. This plot of $E(\mathbf{k})$ versus $\mathbf{k}$ is known as a dispersion diagram. For example, the band gap in Si is 1.1 eV, but the energy of most electrons in this material is somewhat smaller. We now follow the same approach to represent pictorially what we described in equations in Chapters 13 and 14. Remember that the difference to the solid-state physics approach is that, in TEM, the energy of the electrons is ≥ 100 keV.

In this chapter we will see the real origin of the extinction distance ξ_g, which we introduced in equation 13.4. We will discuss how it relates to particular materials and why it varies with the diffraction vector being used. We will then discuss the physical origin of the concept of the effective extinction distance, i.e., the value which the extinction distance appears to have when $s \neq 0$. This discussion of dispersion surfaces is included as a separate chapter, so that you can omit it without affecting your understanding of the rest of the text. We should give you a warning: this is a subject which has probably turned off many potential microscopists. It can be very mathematical, pure theoretical physics, or it can provide many useful insights into image formation. We are trying for the latter. If we aren't completely successful, take heart; many established microscopists have survived without completely mastering this concept!

The dispersion surface is a pictorial representation of the relationship between **k** and energy.

D. B. Williams et al., *Transmission Electron Microscopy*

Dispersion Surfaces

15

15.1. INTRODUCTION

The analysis of Bloch waves as they apply to electrons in solids is well documented in the solid-state literature. However, what we want from the theory is different than what an electrical engineer might want: we want to understand how it applies to the formation of contrast in TEM images and DPs. With this aim in mind, we will again follow the treatment given in Metherell's classic and well-hidden article, already referenced in Chapters 13 and 14. In Chapter 14, we derived equations relating $\mathbf{k}$ to $U_{\mathbf{g}}$. (See Section 14.2 for the definition of $U_{\mathbf{g}}$.) Specifically, we found that there are two Bloch waves if there are two Bragg beams, $\mathbf{0}$ and $\mathbf{g}$. We can rewrite equation 14.35 incorporating equation 14.32 as

$$\frac{C_{\mathbf{g}}^{(j)}}{C_{\mathbf{0}}^{(j)}} = \frac{\left(k^{(j)}\right)^2 - \mathcal{K}^2}{U_{-\mathbf{g}}} = \frac{U_{\mathbf{g}}}{\left(k^{(j)} + g\right)^2 - \mathcal{K}^2} \qquad [15.1]$$

where $C_{\mathbf{0}}^{(j)}$ is the amplitude of the plane wave with wave vector $\mathbf{k}^{(j)}$, and $C_{\mathbf{g}}^{(j)}$ is the amplitude of the plane wave with wave vector $\mathbf{k}^{(j)} + \mathbf{g}$. The Bloch wave was given in equation 14.12 as

$$b^{(j)}(\mathbf{r}) = \sum_{\mathbf{g}} C_{\mathbf{g}}^{(j)} e^{2\pi i\left(\mathbf{k}^{(j)} + \mathbf{g}\right)\cdot \mathbf{r}} \qquad [15.2]$$

Equation 15.1 says that the values of $C_{\mathbf{g}}^{(j)}$ and $C_{\mathbf{0}}^{(j)}$ are directly related to $k^{(j)2} - \mathcal{K}^2$, and thus to $k^{(j)} - \mathcal{K}$.

In the general many-beam case (actually, in any situation where we have more than two beams), the situation is more complicated. However, we can separate the problem into two parts:

- Determine all the allowed wave vectors $\mathbf{k}^{(j)}$ in a crystal, including all possible orientations.
- Determine which set of the allowed $\mathbf{k}^{(j)}$ wave vectors is actually present when you fix the orientation of your crystal.

The first statement fixes the total energy of the electron and selects the crystal. The second statement applies the boundary conditions for the particular situation you are considering, as we'll illustrate in Sections 15.5 and 15.6.

The solution to the first part of the problem is found by setting $|A^{(j)}| = 0$. (We defined $A^{(j)}$ in Section 14.3 and gave an expression for it in Section 14.5.) If you multiply out the determinant, you get

$$A_{2n}\left(\mathbf{k}^{(j)}\right)^{2n} + A_{2n-1}\left(\mathbf{k}^{(j)}\right)^{2n-1} + \cdots = 0 \qquad [15.3]$$

The coefficient A_n depends on $\mathcal{K}^2$ (i.e., the energy) and $\mathbf{g}$ (i.e., the crystal).

So, the polynomial in $\mathbf{k}^{(j)}$ relates $\mathbf{k}^{(j)}$ to the total energy. This is a dispersion relation as we defined the term in Section 14.4. The equation has $2n$ roots and some might be complex. To quote Metherell, "at first sight therefore, the situation appears to be a complicated one!" So in following Metherell we make two simplifications:

- We consider only the high-energy case.
- We assume that we only excite reflections in the ZOLZ.

There are three reasons for reminding you of these simplifications:

- If you want to make a Bloch-wave calculation where you include more than two Bragg beams, then you will need a computer.
- The diagrams we're considering in this chapter are a pictorial representation. The diagrams help us think about what is actually happening to the Bloch waves. If we just did the calculation, we would lose the physical "feel" for the problem.
- None of the diagrams we draw will consider HOLZ reflections; if we make the beam energy high enough, we don't need to consider them.

However, the energy is not really that high and HOLZ reflections are not only seen experimentally, but can also provide valuable information, as we'll see in Chapters 20 and 21. The saving factor is that modern computers have no problems in handling these equations, especially since they are so amenable to matrix manipulation.

15.2. THE DISPERSION DIAGRAM WHEN $U_g = 0$

When the electrons are in the vacuum, i.e., outside the specimen, the Fourier coefficients, U_g, are 0. We start with equation 14.34, namely,

$$\left(\left|\mathbf{k}^{(j)}\right| - \mathcal{K}\right)\left(\left|\mathbf{k}^{(j)} + \mathbf{g}\right| - \mathcal{K}\right) = \frac{|U_g|^2}{4\mathcal{K}^2} \qquad [15.4]$$

Remember that this equation was derived for the two-beam case. When $U_g = 0$, the left side of this equation is zero and the equation has two solutions.

$$\mathcal{K} = \left|\mathbf{k}^{(j)}\right| \quad \text{or} \quad \mathcal{K} = \left|\mathbf{k}^{(j)} + \mathbf{g}\right| \qquad [15.5]$$

where j is 1 or 2. If we plot out these two solutions we find, as shown in Figure 15.1, that we have two interpenetrating spheres, since both $\mathbf{k}_I$ and $\mathbf{k}_D$ can lie in any direction. Since these two $\mathbf{k}$ vectors have the same length, the two spheres

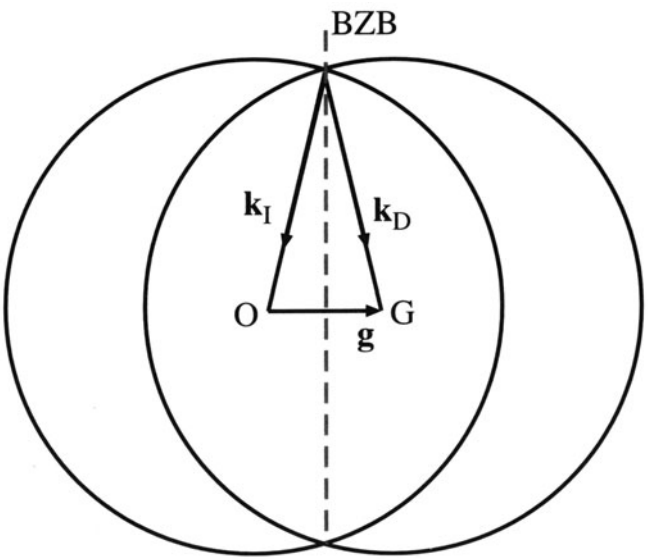

Figure 15.1. Cross section through two spheres of radii $\mathbf{k}_I$ and $\mathbf{k}_D$ centered on O and G, respectively. The spheres represent surfaces of constant energy and the dotted line is the trace of the diffracting plane (and is also equivalent to the Brillouin-zone boundary).

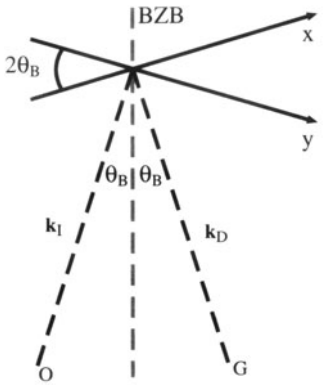

Figure 15.2. An enlarged view of the intersection of the two dispersion spheres at the Brillouin-zone boundary. The projections of the two dispersion surfaces approximate to straight lines x and y, which are normal to $\mathbf{k}_D$ and $\mathbf{k}_I$, respectively.

represent surfaces of constant energy, called dispersion surfaces, one centered on O and the other centered on G.

Of course, we already know that the energy of the electron in a vacuum is related to its wave vector by

$$E = \frac{p^2}{2m} = \frac{h^2\chi^2}{2m} \qquad [15.6]$$

where $\boldsymbol{p}$, the momentum, is related to the wave vector in a vacuum, χ, by $\boldsymbol{p} = h\chi$. Here, χ is the $\mathbf{k}$ when the electron is in a vacuum.

Rearranging, we have

$$\chi = \left\{\frac{2m}{h^2}E\right\}^{\frac{1}{2}} \qquad [15.7]$$

The dotted line drawn in Figure 15.1 represents a plane which is defined by the circle created by the intersecting spheres. In solid-state physics this plane is known as the Brillouin-zone boundary (BZB).

While you work through the diagrams in this chapter, you must remember that for high-energy electrons the scattering angles, e.g., $2\theta_B$, are usually small and the region of interest in reciprocal space is, therefore, close to the BZB. We can redraw part of Figure 15.1 to show an enlarged view of the region close to the BZB in Figure 15.2. At high energies, we approximate the surfaces as a pair of straight lines in projection because λ is very small.

15.3. THE DISPERSION DIAGRAM WHEN $U_g \neq 0$

When $U_g \neq 0$ we know from equation 15.4 that $\mathcal{K}$ can never be equal to $|\mathbf{k}_I|$ or $|\mathbf{k}_D|$. Since equation 15.4 is quadratic we

must have two values for |**k**|. So, the two "spheres" can't intersect if $U_g \neq 0$. We notice that equation 15.4 resembles that for a hyperbola, $xy = a$, where the x and the y axes are shown in Figure 15.2. We can draw these two hyperbolae with their asymptotes as shown in Figure 15.3. These surfaces (remember we are in three dimensions) are known as *branches* of the dispersion surface. The upper branch corresponds to $\mathbf{k}^{(1)}$ and the lower to $\mathbf{k}^{(2)}$. We now have vectors $\mathbf{k}^{(1)}$ and $\mathbf{k}^{(2)}$ where we used to have $\mathbf{K}_I$ and $\mathbf{K}_D$. There are some critical points to remember in this discussion from Chapters 13 and 14:

- The Bloch wave $b^{(1)}(\mathbf{k}^{(1)}, \mathbf{r})$ is associated with $\mathbf{k}^{(1)}$.
- The Bloch wave $b^{(2)}(\mathbf{k}^{(2)}, \mathbf{r})$ is associated with $\mathbf{k}^{(2)}$.
- The intensity of the Bragg beam is a function of thickness, $|\phi_g(t)|^2 \propto \sin^2(\pi t \Delta k)$ (from equation 13.45).

The difference between Figures 15.1 and 15.3 is the gap between the two branches in Figure 15.3. This gap is present because U_g is not zero; U_g is not zero because we have a periodic array of atoms, i.e., a crystal. This gap is directly analogous to the band gap in semiconductor theory where there are forbidden electron energies within the crystal.

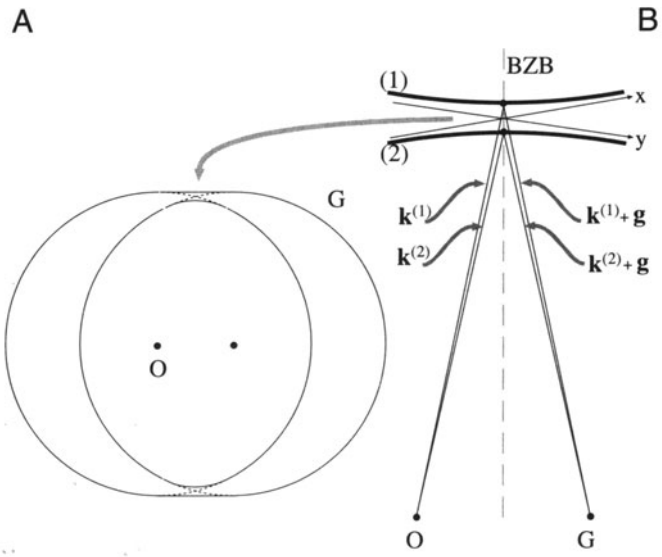

Figure 15.3. When the electron is inside the specimen (i.e., $U_g \neq 0$) and there are two values of **k**, the two dispersion spheres can't intersect and two branches of the dispersion surface, (1) and (2), are created: (A) and (B) show the nonintersecting spheres and an enlarged view showing pairs of vectors, $\mathbf{k}^{(1)}$ and $\mathbf{k}^{(2)}$, and $\mathbf{k}^{(1)} + \mathbf{g}$ and $\mathbf{k}^{(2)} + \mathbf{g}$.

15.4. RELATING DISPERSION SURFACES AND DIFFRACTION PATTERNS

We can gain a lot of physical insight into Bloch waves using the dispersion-surface construction rather than solving the Bloch-wave equations on the computer. Our approach is relatively simple: we start with the dispersion surface shown in Figure 15.4A and draw an initial line to represent the incoming beam traversing the thin foil. We start by assuming an idealized thin specimen with parallel surfaces. We then draw a line normal to any surface that the initial line encounters. This allows us to match the components of wave vectors parallel to that surface.

This is the wave matching construction.

Finally, we extend the points M_1 and M_2 back to the χ spheres in Figure 15.4B. The last part of the process is always to relate the waves in the crystal to the beams in the vacuum, since our recording film, etc., is always outside the crystal.

In this discussion, we will limit ourselves to the two beams, O and G. As we know from Section 13.8, the only values of C (the coefficients of the Bloch waves) which will then be nonzero are $C_{\mathbf{0}}^{(1)}$, $C_{\mathbf{0}}^{(2)}$, $C_{\mathbf{g}}^{(1)}$, and $C_{\mathbf{g}}^{(2)}$.

First, we need to know which points on the dispersion surface will actually correspond to the diffraction condition we have chosen. Next, we need to know the orientation of the specimen relative to the beam and the orientation of the Bragg planes.

We begin by considering the case where the surface of the specimen is parallel to **g**; we will explain why we are so specific on this point in a moment.

Now we have fixed the specimen and **g**. If we align the incident beam parallel to the $(hk\ell)$ planes, then we will excite points M_1^B and M_2^B on separate branches of the dispersion surface shown in Figure 15.4A. The extinction distance will then correspond to Δk^{-1} for $s = 0$, as in Section 13.10. If we now tilt the incident beam so that χ moves closer to the vertical (keeping the specimen fixed), then the excited points become M_1, and M_2 and, as we see in Figure 15.4, s becomes negative.

We define the lines $M_1^B M_2^B$ and $M_1 M_2$ to be *tie lines* because they tie together points on the different branches of the dispersion surface. Both tie lines are parallel to the BZB, because we chose the top surface of the specimen to be parallel to **g**.

Each of these tie lines is normal to the surface which produces it.

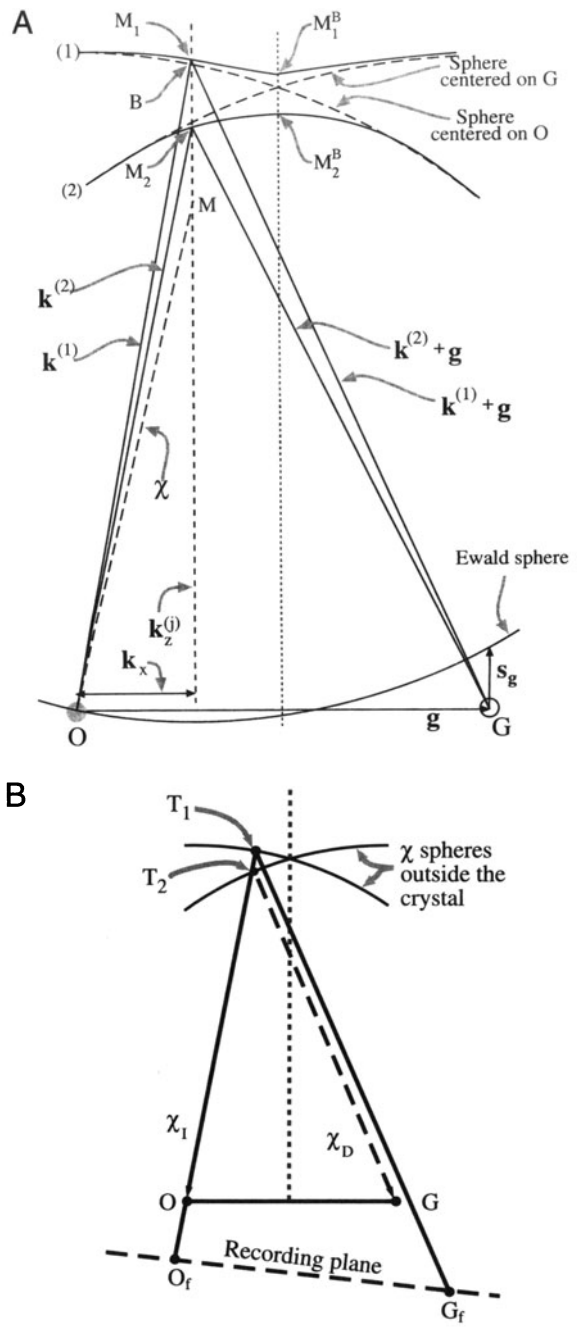

Figure 15.4. (A) Combination of the dispersion surfaces (1) and (2), centered on O and G, with the Ewald sphere construction. The surface of the specimen has been set to be parallel to **g**, so points M_1^B and M_2^B on the branches (1) and (2) are excited. The incident beam direction is given by the vector **MO**. If we tilt the beam so χ (as shown) becomes more vertical, the excited points move to M_1 and M_2 giving the tie line M_1M_2. The vectors $\mathbf{k}^{(1)}$ and $\mathbf{k}^{(2)}$ start at M_1 and M_2, respectively, and end on O. (B) Extension of the lines OM_1 and OM_2 in (A) back to the χ spheres at T_1 and T_2, respectively, relates the waves in the crystal to the beams outside. The points O_f and G_f are what you record on the photographic film.

As shown on the enlarged view in Figure 15.5, each of the **k** vectors has an associated wave amplitude $C_{\mathbf{g}}^{(j)}$ associated with it.

The diagrams of the dispersion surface in Figures 15.4 and 15.5 contain lots of reminders:

- For this orientation, $\mathbf{k}_x$ is the same for all **k** vectors ending on O.
- You can recognize $\gamma^{(1)}$ and $\gamma^{(2)}$ from Section 13.7.
- The vacuum wave vector χ is always shorter than $\mathcal{K}$ or **k.**

We can understand these changes from the following argument. The O beam is always excited, so $C_0^{(1)}$ and $C_0^{(j)}$ will always be relatively large. Which other values of C are large will depend on where the Ewald sphere cuts the systematic row of relrods.

Now we can consider what happens when the surface of the specimen is *not* parallel to **g**. Here, the normal to the surface, **n**, is not parallel to the BZB. However, the tie line is always parallel to **n** so the tie line is no longer parallel to the BZB. Remember: this construction matches the components of the **k** vector which are parallel to the surface of the specimen. We saw this clearly in Figure 15.4, where we commented that $\mathbf{k}_x$ is the same for all the vectors ending on O because we chose the beam to be normal to the surface in that case.

> The tie line is a graphical method of satisfying the boundary conditions imposed by the TEM specimen.

We don't need tie lines in solid-state physics if the electrons are always moving in a perfect lattice where we don't consider surfaces.

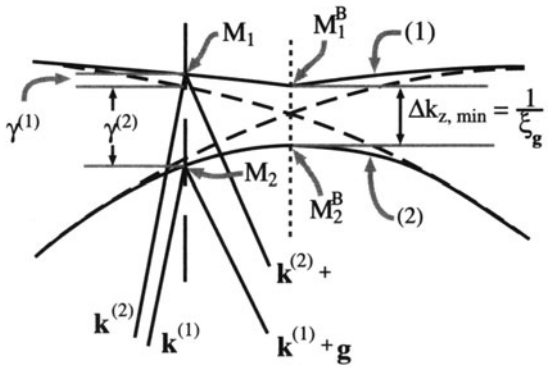

Figure 15.5. An enlarged region of Figure 15.4A showing how the vectors $\mathbf{k}^{(1)}$ and $\mathbf{k}^{(2)}$ are related to the quantities $\gamma^{(1)}$ and $\gamma^{(2)}$ and the distance Δk_z.

We are now ready to consider the more common TEM wedge specimen shown in Figure 15.6A and then we'll see how these excited Bloch waves relate to the DP.

The wedge has been drawn with the top surface parallel to **g**. Thus we have tie line $\mathbf{n}_1$. When the electrons exit the crystal at the inclined bottom surface, we again match components parallel to this surface so we have tie line $\mathbf{n}_2$. Notice that we must draw $\mathbf{n}_2$ through both M_1 and M_2. These tie lines don't excite extra points on the dispersion surface because we are leaving the crystal.

Once we're outside the crystal, we know that the wavelength must be χ and that χ defines a pair of spheres centered on O and G. So we extend the $\mathbf{n}_2$ tie lines until they reach the χ spheres. Now we have excited four points, as we see graphically in Figure 15.6A. The points on the O circle are labeled O_1 and O_2; those on the G circle are D_1 and D_2. We have labeled the subscripts this way because they correspond to the plane waves $\chi_0^{(1)}$, $\chi_0^{(2)}$, etc., as also shown in Figure 15.6A.

Now we have reached the final step: we have to relate these beams to the DP. Yes, they are real beams because we are now outside the specimen and in a vacuum. We show this in Figure 15.6B. All of the χ beams have been related to point O_1 because $\chi_0^{(1)}$ is the direct beam. Remember: $\chi_0^{(1)}$ is not vertical because **g** is horizontal. The vectors $\chi_0^{(1)}$ and $\chi_0^{(2)}$ are not parallel because they are both radii of the circle χ_0 and originate at different points on the circle.

The conclusion is that we will have two spots at O and two spots at G. In other words, the fact that we have a wedge specimen has split the spots at G. We will see these split spots in Chapter 18 and we will return to this topic in Chapter 23, when we discuss images.

It can be useful to extend the wedge case to the double wedge. For example, imagine an inclined planar defect in a parallel-sided slab with **g** parallel to the slab surface, as shown in Figure 15.7. Everything is as before at the top surface. At the inclined interface then, tie lines do create new excited points B_1 and B_2 on the 1 and 2 branches of the dispersion surface.

Now, $\mathbf{n}_3$ is the tie line due to the bottom surface and $\mathbf{n}_3$ is parallel to $\mathbf{n}_1$. We extend the $\mathbf{n}_3$ tie lines to the χ spheres and find that now we have three χ_0 vectors and three χ_D vectors. Translating these χ vectors to O_1 as the common origin produces the beam diagram shown in Figure 15.7B. Now we have three spots at O and three spots at G. We will return to this topic in Chapter 24 when we discuss images of planar defects, but here let's summarize the new concepts they give us:

- The dispersion surface is a graphical approach to thinking about Bloch waves.

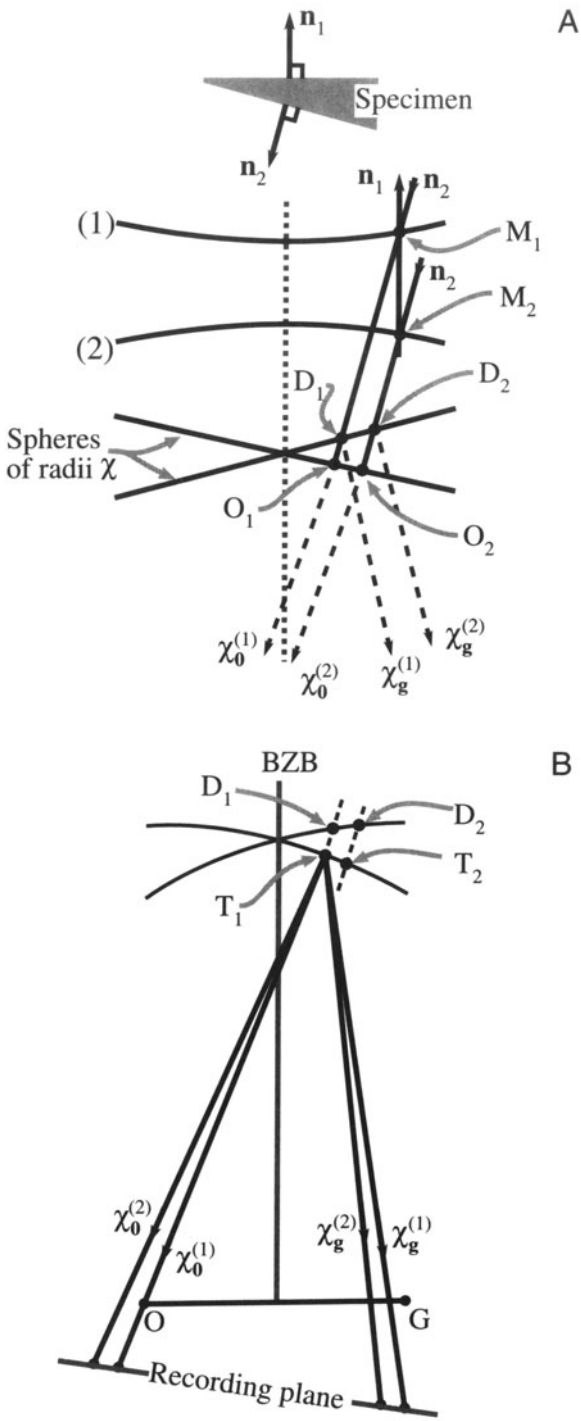

Figure 15.6. (A) The same diagram as Figure 15.4B, but for a wedge specimen with top surface parallel to **g** (normal $\mathbf{n}_1$) and the bottom surface normal $\mathbf{n}_2$. Instead of exciting two points, O_1 and O_2, we excite two more, D_1 and D_2, which correspond to the plane waves $\chi_0^{(1)}$, $\chi_0^{(2)}$, outside the crystal. In (B) we relate all the beams to the point O_1 and we produce two beams at O and two at G. Thus we can predict that a wedge foil will give doublets at O and G.

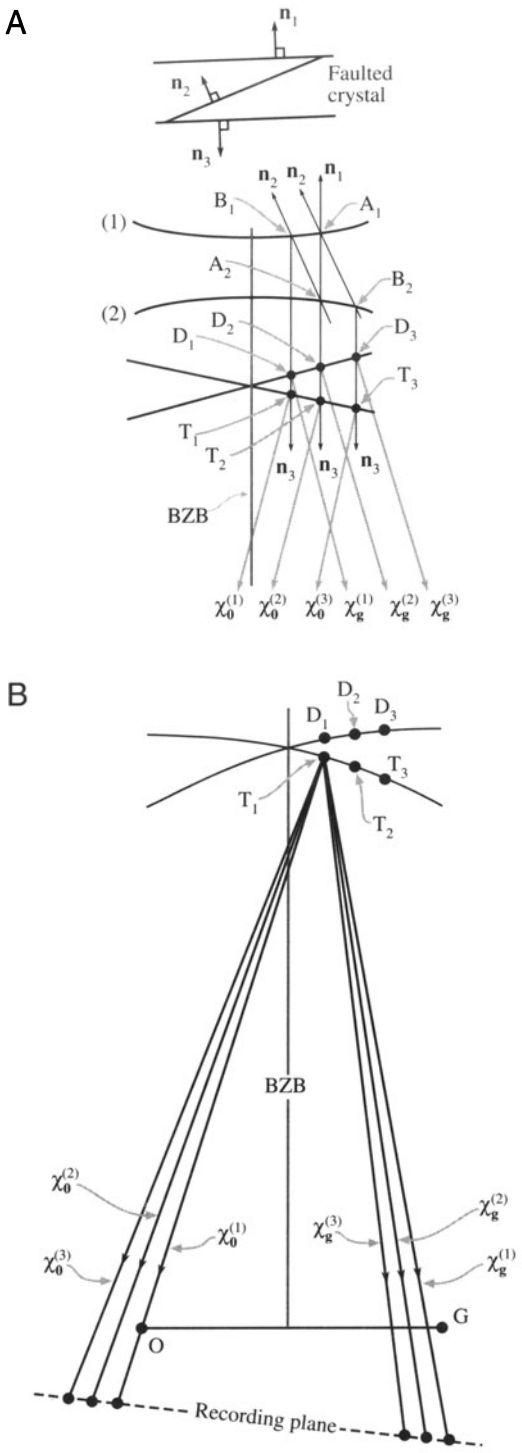

Figure 15.7. (A) An enlarged view of the dispersion surface in Figure 15.6 close to the BZB, but this time for a specimen in which both surfaces are parallel to **g** but there is an inclined fault which produces a third wave $\chi_0^{(3)}$ and $\chi_g^{(3)}$. (B) If we then move all the vectors to O_1 again, we predict there will be three spots at O and three at G.

- We have to match the components of any wave entering and leaving any surface, internal or external.
- We use the exit-surface tie line to link to the χ spheres.
- Having two inclined surfaces causes a splitting of the Bragg beams.
- An internal interface, such as a stacking fault, increases the number of points excited on the dispersion surfaces.

To understand the importance of these ideas, try to imagine what will happen when a defect, which is not abrupt, is present in the crystal (more on this in Section 15.8).

15.5. THE RELATION BETWEEN U_g, ξ_g, AND s_g

We can best appreciate the importance of the dispersion-surface construction by looking at Figure 15.4. This figure shows the original spheres as dashed lines: they are nearly flat close to the BZB. The electron beam is initially traveling with wave vector χ outside the crystal. When the beam enters the crystal the z component of this wave vector changes (i.e., the refraction effect we saw in Chapters 11 and 13), but the xy component is unchanged. Therefore, the allowed **k** vectors in the crystal are $\mathbf{k}^{(1)}$ and $\mathbf{k}^{(2)}$. One **k** vector begins on branch 1 and ends at O, while the other begins at branch 2 and ends at O.

Aside: There are only two **k** vectors because there are only two branches of the dispersion surface. There are two branches of the dispersion surface because we are considering only two beams. Clearly, we can draw in $\mathbf{k}_{\mathbf{g}}^{(2)}$ and $\mathbf{k}_{\mathbf{g}}^{(1)}$ by adding **g**. Now, how does $\mathbf{k}_{\mathbf{0}}^{(1)}$, say, relate to **K**? The point K is also determined by the tie line through χ, and lies on the circle centered on O. Most importantly, neither $\mathbf{k}_1$ nor $\mathbf{k}_2$ is equal to $\mathcal{K}$. If you look back at equation 13.41 you can see that

$$\mathbf{k}_z^{(i)} - \mathcal{K}_z = \gamma^{(i)} \qquad [15.8]$$

So $\gamma^{(i)}$ is simply the distance of the point M_j from the $\mathcal{K}$ sphere centered on O. We can write this relationship explicitly

$$\mathbf{k}^{(i)} = \mathbf{k}_z^{(1)} + \mathbf{k}_x^{(i)} \qquad [15.9]$$

$$= \left(K_z + \gamma^{(i)}\right)\mathbf{u}_z + \mathrm{k}_x\mathbf{u}_x \qquad [15.10]$$

Notice that the last term here is independent of i. Look again at Figure 15.4. You can see that Δk_z is a minimum when M_1 and M_2 lie on the BZB. In that situation

$$\Delta k_{z\,\min} = \gamma^{(1)} - \gamma^{(2)} \qquad [15.11]$$

Simply by looking at the diagram, and as expected from Chapter 13, you also know that

$$\gamma^{(1)} - \gamma^{(2)} = \frac{U_g}{k} = \frac{1}{\xi_g} \qquad [15.12]$$

So

[15.13]

The origin of the thickness oscillations is the difference in wavelength of the two Bloch waves. It's the beating between the two Bloch waves.

Thus you see that the gap Δk_z at the BZB is given by the reciprocal of the extinction distance.

- We have a crystal, therefore $U_g \neq 0$.
- Since $U_g \neq 0$, we have two branches to the dispersion surface and hence a band gap.
- The band gap is Δk_z.
- Hence we have a finite extinction distance (i.e., ξ_g is not infinite).

An aside: think how s_{eff} and s would be related if ξ_g were infinite. (Go back to equation 13.47.)

If the tie line M_1M_2 does not lie on the BZB, then when we draw the Ewald sphere centered just below M_1 (with radius of length $1/\lambda$ or $|\mathcal{K}|$) we see that s_g is nonzero. We can easily see from the equations in Section 13.10 that, in general, Δk_z is given by

$$\Delta k_z = s_{\text{eff}} = \frac{1}{\xi_{\text{eff}}} \qquad [15.14]$$

This equation is the key to understanding the origins of the extinction distance and why the effective extinction distance depends on the size of the excitation error, **s**. It says that the band gap increases as we increase **s**. Looking at it another way, as we move the tie line off the BZB, the band gap $\Delta\mathbf{k}$ increases.

Some questions raised here are:

- What is the physical reason that Δk_z is related to **s**?
- What happens if **g** is not parallel to the foil surface or, indeed, if the foil surfaces are not parallel to one another?

15.6. THE AMPLITUDES OF BLOCH WAVES

In Section 13.9, we found that the total wave function for the two-beam case can be expressed as the sum of two Bloch waves

$$\psi(\mathbf{r}) = \mathcal{A}^{(1)}b^{(1)} + \mathcal{A}^{(2)}b^{(2)} \qquad [15.15]$$

The relative contributions of the two Bloch waves, $\mathcal{A}^{(1)}$ and $\mathcal{A}^{(2)}$, were shown to be cos β/2 and sin β/2, respectively, and $w = \cot\beta = s\xi_g$.

We also showed in Section 13.8 that

$$b^{(1)}\left(\mathbf{k}^{(1)},\mathbf{r}\right) = C_0^{(1)}e^{2\pi i\,\mathbf{k}^{(1)}\cdot\mathbf{r}} + C_g^{(1)}e^{2\pi i\,(\mathbf{k}^{(1)}+\mathbf{g})\cdot\mathbf{r}} \qquad [15.16]$$

and

$$b^{(2)}\left(\mathbf{k}^{(2)},\mathbf{r}\right) = C_0^{(2)}e^{2\pi i\,\mathbf{k}^{(2)}\cdot\mathbf{r}} + C_g^{(2)}e^{2\pi i\,(\mathbf{k}^{(2)}+\mathbf{g})\cdot\mathbf{r}} \qquad [15.17]$$

The Bloch-wave coefficients were given by equation set 13.31

$C_0^{(1)}$	$C_0^{(2)}$	$C_g^{(1)}$	$C_g^{(2)}$
cos β/2	sin β/2	–sin β/2	cos β/2

Now we can consider some special cases and examine the actual values for $C_0^{(1)}$, $\mathcal{A}^{(1)}$, etc. (Table 15.1).

For the Bragg case, $s_g = 0$, **g** is exactly excited and $\mathcal{A}^{(1)}$ and $\mathcal{A}^{(2)}$ are both equal to $1/\sqrt{2}$. In other words, the two Bloch waves are equally excited.

For the case where $s_g < 0$, we now have cos (β/2) > sin (β/2) so that $\mathcal{A}^{(1)}$ is greater than $\mathcal{A}^{(2)}$. If we reverse the sign of **s**, cos (β/2) < sin (β/2) and $\mathcal{A}^{(1)}$ is less than $\mathcal{A}^{(2)}$.

The result is that whether Bloch wave 1 or Bloch wave 2 has the larger amplitude depends on the sign of **s**.

Now, let's relate this information to the dispersion surface shown in Figure 15.4. When $s_g < 0$, as shown here, the M_1M_2 tie line is to the left of the BZB, which is associ-

Table 15.1. Values of Bloch-Wave Variables

s	w	β	β/2	cos (β/2)	sin (β/2)
0	0	π/2	π/4	$1/\sqrt{2}$	$1/\sqrt{2}$
+0.01	+Δ	π/2 – δ	π/4 – δ/2	$1/\sqrt{2} + \varepsilon$	$1/\sqrt{2} - \varepsilon$
–0.01	–Δ	π/2 + δ	π/4 – δ/4	$1/\sqrt{2} - \varepsilon$	$1/\sqrt{2} + \varepsilon$

ated with reflection G. When the tie line is closer to O than G, Bloch wave 1 is more strongly excited; the reverse is true when the tie line crosses the BZB. We should remember that the analysis in Chapter 13 was for a two-beam case, where we were close to the Bragg condition. So the discussion of $\mathcal{A}^{(1)}$ and $\mathcal{A}^{(2)}$ only applies to small values of **s**.

15.7. EXTENDING TO MORE BEAMS

If we allow more beams to contribute to the image, we can picture the dispersion surface for the case where $U_g = 0$ by constructing more spheres, shown in Figure 15.8. If we have n beams, then we will have n spheres. Note that each sphere is centered on its corresponding reciprocal lattice point and neighboring spheres intersect periodically spaced BZBs. The gap in Figure 15.3 always occurs at the BZB. The BZB itself always corresponds to a plane which is the perpendicular bisector of a **g** vector. Thus the diagram for >2 beams shown in Figure 15.8 will become more complicated with many band gaps and many branches, as shown in Figure 15.9. The band gap tends to decrease as the rank of the neighboring branches decreases.

In Chapter 26, we'll discuss what happens in images when 3**g** is excited. We will actually consider the two-beam condition, where **0** and 3**g** are the two beams.

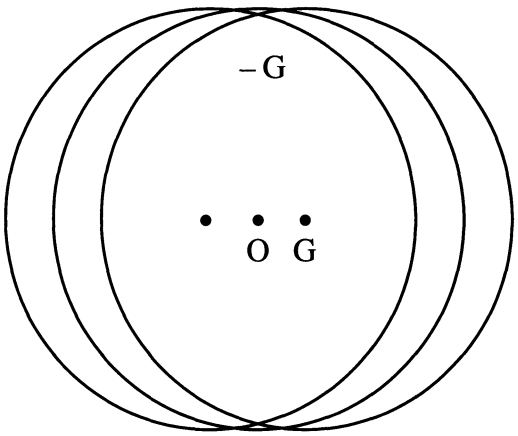

Figure 15.8. Three dispersion spheres due to three reflections, -G, O, and G. If we had n spots we would have n spheres.

We follow the convention used by Metherell (1975) and number the branches of the dispersion surface from the top down. Then $i = 1$ corresponds to the branch with the highest kinetic energy. Remember that all the electrons have the same total energy in this treatment. You must also be aware that some earlier texts number the top branch two and the second branch one, following Hirsch *et al.* (1977). This was fine when only two branches were considered.

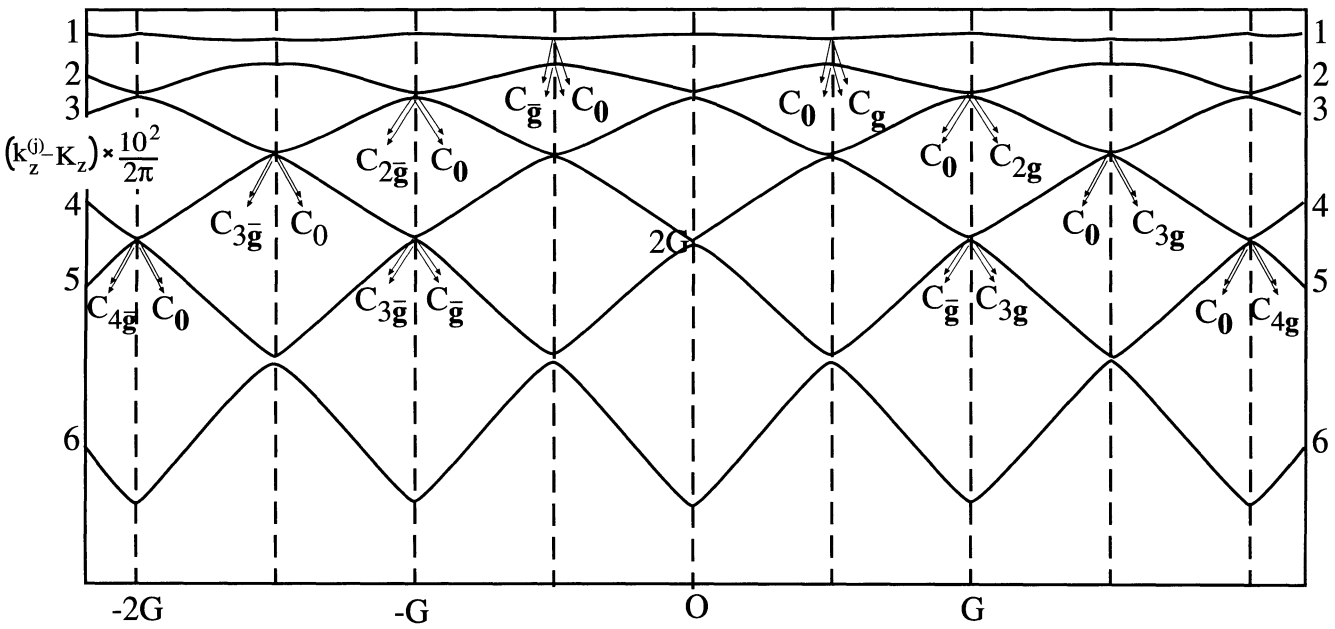

Figure 15.9. Six branches of the dispersion surfaces. The two branches $i = 1$ and $i = 2$ have the highest energy and give the largest band gap; notice that these branches give the terms in C_0 and C_g; smaller gaps occur between branches with lower energy. The diagram can be approximated to a set of spheres centered on O, ±G, and ±2G, etc.; C_0 is "normal" to the sphere centered on O, while C_g is "normal" to the sphere centered on **g**, etc.

We can still associate the amplitudes C_0, C_g, etc. with the sphere centered on **0**, **g**, etc. The result is shown by the labels C_0, C_g, etc. in Figure 15.9. For example, imagine the original spheres centered on **0** and **g**; they intersect on the BZB which passes through **g**/2, so the C_0, C_g are labeled as shown.

Similarly, the spheres centered on **0** and 3**g** intersect on the BZB which passes through 3**g**/2, so C_0, C_{3g} are labeled. As a general rule, C_{ng} will be largest for the pair of reflections which are excited, i.e., **0** and n**g**, and will be located on the n**g**/2 BZB.

We now extend these arguments to the situation where many beams are excited. Values of C other than C_0 and C_{ng} will be nonzero, since it's no longer a two-beam case. So the tie line M_1M_2 will then intersect many branches of the dispersion surface. The reason these contributions are smaller when **g** is excited is that they do not intersect the **0** circle. However, they can contribute to the image. Figure 15.9 shows how this can be visualized. (Remember, the dispersion surface is a way of visualizing Bloch-wave coefficients.) If we satisfy reflection 2G, then $C_{\mathbf{0}}^{(1)}$, $C_{\mathbf{0}}^{(2)}$, $C_{\mathbf{0}}^{(1)}$, $C_{2\mathbf{g}}^{(1)}$, and $C_{2\mathbf{g}}^{(2)}$ are all large. The gap $\Delta k_{4,5}$ between branch 4 and branch 5 at G (on the BZB) is small; the "circles" would have intersected in the vacuum. If we think about the Ewald sphere, we can show that the **s** values for $\bar{\mathbf{g}}$ and 3**g** are identical. We'll see later (Chapter 26) that these reflections will actually couple strongly, although both are weakly excited and the extinction distance is large (because the gap $\Delta k_{4,5}$ is small). The extinction distance for the coupling of **g** and 3**g** when 2**g** is strongly excited is $\xi_{4\mathbf{g}}$ ($\xi_{3\mathbf{g}-(-\mathbf{g})}$). We can see this is true by looking at the branch 4/5 gap on the G BZB.

15.8. DISPERSION SURFACES AND DEFECTS

The original reason for introducing the concept of Bloch waves was that only Bloch waves can exist in a periodic potential, i.e., there are no beams in the crystal. So what happens when a defect is present? We'll discuss this situation in some detail in Chapters 23–26 but will mention the basic ideas here, emphasizing the Bloch waves rather than the defects.

In Section 15.4, we discussed the effect which a stacking fault can have on the Bloch waves using the dispersion surface representation. What we were actually doing was matching the components parallel to the planar defect, so the effect of the stacking fault was to create new tie lines $\mathbf{n}_2$. The general result is that when a defect is present, energy is transferred from one Bloch wave to the other along the tie line; this is known as *interband scattering*. This concept is not only important for our understanding of images of planar defects, but also illustrates a general principle for defects.

The difficulty with nonplanar defects is that the tie lines are not so well defined. You can, however, imagine the result: instead of having points on the dispersion surface, we will have a distribution of points. We then relate this distribution to the DP. We do this with the tie lines normal to the exit surface and then translate to O_1 in the usual way. So, our distribution of points on the dispersion surface will become a distribution of spots in the DP; this distribution is what we will call a streak in Chapter 17.

CHAPTER SUMMARY

Dispersion surfaces allow us to draw diagrams to represent the equations given in Chapter 14. These surfaces are essentially plots of the **k** vector of the Bloch waves (which is directly related to the energy) versus the $\mathcal{K}$ vector. They correspond directly to the band diagrams, which are used extensively to represent energy levels in semiconductors; the difference is that, in semiconductors, we emphasize energy by plotting energy versus reciprocal-lattice vector (our $\mathcal{K}$ vector). The **k** vectors themselves vary because, although the total energy of each electron is a constant, the potential energy decreases when the electron is close to the nucleus, causing the kinetic energy to increase.

The most important equation is 15.14, which relates Δk_z, s_{eff}, and ξ_{eff}. Notice that Δk_z is defined for two Bloch waves but is only small when the Bragg equation is nearly satisfied. This relationship links Bloch waves and Bragg beams. Δk is only nonzero because we have a crystal. Δk gives rise to thickness fringes and all thickness effects. Thus we see that thickness variations are due to the interference, or beating, of pairs of Bloch waves. As we increase n, ξ_g increases because the gap between the two relevant branches of the dispersion surface becomes narrower. Defects present in the crystal cause a mixing or coupling of the Bloch waves: they "tie" the branches of the dispersion surface and cause interband scattering.

We've emphasized throughout this chapter that the dispersion surface is a pictorial representation of the $\mathbf{k}$ versus $\mathcal{K}$ relationship. We'll close by quoting the result derived by Kato (1957).

> In any wave field, the direction of energy flow is along the normal to the surface of the dispersion surface. This result is equally valid for "electron wave packets" and other waves. The physicist might say that the Poynting vector is normal to the dispersion surface.

Although there are many texts which discuss dispersion surfaces and band gaps in semiconductors, beware of the $2\pi/\lambda$ versus $1/\lambda$ problem since many of these texts are by, and for, physicists. Defect analysis using Bloch waves has generally been the preserve of the physicist. However, there are some excellent programs available which use a Bloch-wave approach analysis.

We give the usual caveat: beware of black boxes. Metherell's article goes to greater depth than covered here. However, it has been an inspiration for much of this chapter and is highly recommended for advanced study. It is beautifully written and explained, but is certainly more advanced than our text. If you want to delve deeper into this topic, this is *the* article. Note that Metherell uses the e^{ikr} notation.

REFERENCES

General References

Ashcroft, N.W. and Merman, N.D. (1976) *Solid State Physics,* W.B. Saunders Co., Philadelphia. Chapter 8 ($2\pi/\lambda$ is used).

Kittel, C.J. (1986) *Solid-State Physics,* 6th edition, John Wiley & Sons, New York. Chapters 1, 10, and 11 are particularly relevant.

Metherell, A.J.F. (1975) in *Electron Microscopy in Materials Science,* **II**, (Eds. U. Valdrè and E. Ruedl), p. 397, CEC, Brussels. *The* reference.

Specific References

Kato, N. (1958) *Acta. Cryst.* **11**, 885.

Hirsch, P.B., Howie, A., Nicholson, R.B., Pashley, D.W., and Whelan, M.J. (1977) *Electron Microscopy of Thin Crystals,* 2nd edition, Krieger, Huntington, New York. Chapter 9.